Millisecond bidirectional protein translocation by a AAA+ disaggregation machine

Remi Casier[1], Dorit Levy[1], Inbal Riven[1], Yoav Barak[2], Gilad Haran[1]*

[1]Department of Chemical and Biological Physics, Weizmann Institute of Science, Rehovot 761001, Israel

[2]Chemical Research Support, Weizmann Institute of Science, Rehovot, 761001, Israel

Abstract. How biological machines utilize ATP to facilitate mechanical work remains heavily contested. ClpB is a quality control machine of the AAA+ family that salvages misfolded and aggregated proteins by forcibly translocating them through its lumen. Structural studies of this and similar machines have suggested a power-stroke translocation mechanism directly coupled to sequential subunit motion. However, functional studies have challenged this deterministic view. Here, we directly track substrate translocation of individual ClpB hexamers trapped within lipid vesicles. Using single-molecule FRET, we find that translocation occurs in milliseconds, far exceeding ATP hydrolysis rate. We further observe partial substrate engagement events and even translocation proceeding in both directions through ClpB's lumen. Rather than generating discrete power strokes, ATP appears to act by regulating substrate engagement and translocation directionality. These results indicate a fast, stochastic mechanism akin to a *Brownian motor*, redefining how ATP is coupled with mechanical action in AAA+ machines.

Introduction. The ubiquitous superfamily of AAA+ (ATPases associated with diverse cellular activity) proteins participates in essential cellular activities including protein disaggregation and degradation, DNA replication and recombination, organelle biogenesis, and cellular remodeling.[1-3] Despite their remarkable functional diversity, they typically assemble into ring-like hexamers and share conserved nucleotide-binding domains (NBDs) that couple ATP turnover to mechanical work.[3] However, how ATP energy is utilized to promote the activity of these proteins remains under debate. In recent years, a plethora of cryogenic electron microscopy-derived 3D structures of AAA+ machines have been observed, with a particular focus on machines that translocate client proteins through their central lumen for protein quality control activities. Rather than adopting a fully symmetric ring, many of the AAA+ assemblies were shown to form a spiral-like configuration instead.[4-7] These studies have led to the proposed hand-over-hand model for their translocation mechanism, which predicts the sequential motion of the subunits in the spiral structures.[4,8-11] At each step, the top subunit moves down following ATP (adenosine triphosphate) hydrolysis, pulling two substrate protein residues in a *power-stroke-like*[12,13] manner, i.e., ATP hydrolysis directly generates a single forceful translocation step.[8] Yet, biochemical and biophysical studies contest the hand-over-hand model. Experiments on the AAA+ machines ClpA and ClpX demonstrated that they can function in translocating proteins even when up to three of their subunits are defective in ATP hydrolysis,[14,15] ruling out a fully coordinated, sequential subunit motion. Further, optical tweezer experiments found that more than 500 amino-acid (*aa*) residues could be translocated in a second by the AAA+ disaggregase ClpB,[16] suggesting activity that is two orders of magnitude faster than its ATP hydrolysis rate. Studies further pointed to the viable possibility of partial substrate threading by ClpB.[17] Finally, it has been shown that pore loops, which are the substrate-engaging elements

within ClpB's lumen, perform active, nucleotide-dependent up-and-down motion on the sub-millisecond time scale, again much faster than ATP hydrolysis.[18] These observations point to the need for direct observation of translocation to obtain decisive, real-time evidence of the mechanism of action of these machines. Here, we answer this challenge by using single-molecule Förster resonance energy transfer (smFRET) experiments to directly monitor, in real time, the motion of a substrate protein through the lumen of ClpB, a classic disaggregation machine.[19,20] Our experiments demonstrate that substrate translocation occurs in a bidirectional manner on a timescale much faster than the rate of ATP hydrolysis. Instead of a *power-stroke* mechanism, we propose a stochastic, ATP-dependent translocation process. In this process, the consumption of ATP regulates the directionality of substrate diffusion within the lumen. This *Brownian-motor-like* mechanism[12] enables efficient translocation, allowing complete substrate threading with the consumption of just one or two ATP molecules.

Observing substrate translocation events by ClpB. To gain insight into the molecular mechanism of ClpB, we utilized real-time smFRET to monitor translocation events of the model substrate κ-casein, an unstructured protein.[21,22] We inserted individual copies of the fluorescently tagged proteins inside surface-tethered lipid vesicles (Fig. 1a), which afforded several distinct advantages.[23] The confinement into ca. 120 nm diameter vesicles (Fig. S1) created a high local protein concentration (ca. 2 – 3 μM) which facilitated the bimolecular interactions between the weakly associating species ($K_{D,app}$ (ATP) = 0.6 ± 0.1 μM, Fig. S2), while still allowing the proteins to diffuse freely (Fig. S3). The immobilized vesicles also provided extended observation times, limited only by photobleaching of the dyes, allowing us to observe repeated events. The liposomes were prepared from 1,2-dimyristoyl-sn-glycero-3-phosphocholine (DMPC), which remained near its gel-to-liquid crystalline transition at room temperature (22.5 °C), guaranteeing transient membrane defects that allowed permeation of ions such as ATP.[24,25] The rapid and reversible permeability of the liposomes, demonstrated by control experiments (see *liposome permeability* and Fig. S4 in the SI), facilitated maintaining internal ATP levels.

A sample fluorescence trajectory containing multiple events of interaction between ClpB (constituting of 5 wild-type subunits and one subunit labeled at position 359 on its nucleotide-binding domain 1 (NBD1), see Fig. S5) and casein (labeled on only one of the native cysteines, see Fig. S6 for more details) inside a vesicle in the presence of 2 mM ATP is shown in Fig. 1b. In this trajectory, the donor (Cy3B) fluorescence is represented in green and the acceptor fluorescence (CF660R) is shown in red. Most of the time, there is no energy transfer between the dyes as ClpB and casein independently diffuse within the liposome. Occasionally, there are sudden, brief appearances of high FRET efficiency, indicating that casein has entered the lumen of ClpB (blue, Fig. 1b inset). The peaks in FRET efficiency were characterized by the length of the events (τ_{dwell}) and the maximum FRET efficiency values reached (E_{peak}). As illustrated at the top of Fig. 1b, the contour length of casein (ca. 76 nm = 190 *aa* × 0.4 nm / *aa*)[26] far exceeds the ca. 13 nm length of ClpB's lumen (hexameric model based on PDB 1QVR)[27] and the 6 nm Förster radius (R_0) of the dye pair. Therefore, the probed τ_{dwell} does not correspond to the translocation process of the entire chain of casein but rather to a temporal segment during which the acceptor-labeled portion of casein passes close to the donor on ClpB. To help illustrate this, Fig. 1c presents a calculated map of the expected FRET efficiency (ε_{calc}) as the acceptor traverses through the central pore of ClpB. As the fluorescently labeled residue enters the *N*-terminal domain (NTD), ε_{calc} is less than 0.3, depending on the location within the cross-section of the 2 – 3 nm diameter pore. As the dye travels deeper into the pore, ε_{calc} increases, potentially reaching a

value close to unity around the interface between the NBDs. ε_{calc} then decreases as the labeled segment exits the trans side past the NBD2. Thus, τ_{dwell} values represent the time that it takes a contour length of ~18 *aa*'s (where ε_{calc} > 0.5) of casein to pass through ClpB, and E_{peak} corresponds to the minimum proximity between the two labels during an event.

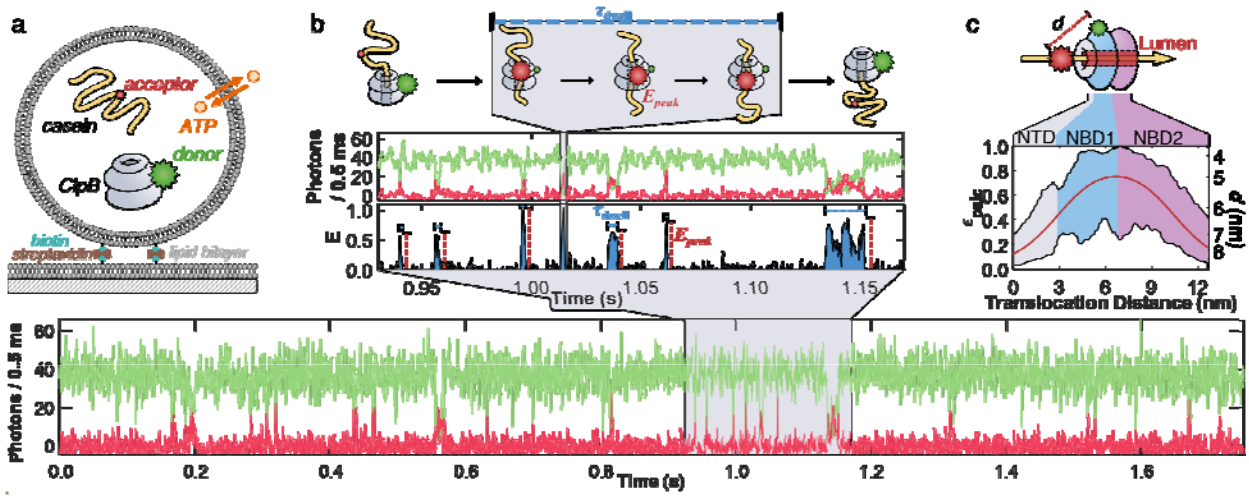

Figure 1. Porus vesicles enable observations of multiple fast events of casein translocation through the lumen of ClpB. a, Schematic overview of a ClpB and substrate-loaded liposome (diameter ca. 120 nm) immobilized on a glass-supported lipid bilayer through a biotin-streptavidin linkage. Only liposomes containing individual copies of a fluorescently labeled ClpB hexamer (grey, with a green donor Cy3b, residue 359) and casein (yellow, with a red acceptor CF660R) were included in the analysis. Liposomes constituting of DMPC remain permeable to ATP (orange) at 22.5 °C, ensuring replenishment of the ATP supply consumed by ClpB. **b,** A sample fluorescence trajectory (bottom) of a ClpB-casein pair inside a liposome in the presence of 2 mM ATP (donor signal, N_D, from ClpB in green, and acceptor signal, N_A, from casein in red). The signals were corrected for background fluorescence and channel crosstalk, see Methods. A zoomed-in region of the trajectory (middle) depicts several short events (characterized by τ_{dwell}) of ClpB and casein interaction through the sudden appearance and disappearance of spikes in the apparent FRET efficiency, E_{app} (= $N_A/(N_D + N_A)$), which reaches a maximum value of E_{peak}. A cartoon (top) illustrates the proposed translocation event of casein through the lumen of ClpB. **c,** A map of the expected FRET efficiency (ε_{calc}) for an acceptor-labeled segment as it passes through ClpB with a donor on residue 359 on the NBD1. The solid red line represents the centerline passing directly through the pore, while the black lines represent the boundaries of the pore (R_0 ~ 6.0 nm). The colored regions correspond to the *N*-terminal domain (NTD, grey) and the two nucleotide-binding domains (NBD1 and NBD2, blue and purple, respectively). The secondary *y*-axis denotes the inter-dye distance (*d*).

smFRET reveals ultrafast translocation of casein. From the sample trajectories given in Figs. 1b and 2a (ClpB labeled on the NBD1), it can be readily seen that the events occur very quickly, lasting only a few milliseconds. The 1535 events measured across 166 trajectories resulted in a power-law distribution of dwell times, τ_{dwell}, $P(\tau_{dwell}) \sim \tau_{dwell}^{-a}$ characterized by a power a =1.69 ± 0.02 (Fig. 2b). Although the τ_{dwell} values spanned several orders of magnitude, the vast majority (89%) of the events took less than 10 ms. Since power laws with powers less than two do not have well-defined means,[28] an estimate of the average dwell time ($<\tau_{dwell}>$) in our experiments was obtained from an exponential fit to the short translocation times constituting the majority of events. The fit revealed a $<\tau_{dwell}>$ value of only 1.6 ± 0.1 ms, nearly 3 orders of magnitude faster than the ATP hydrolysis time of the machine. To preclude the possibility that the short τ_{dwell} values were due to acceptor blinking, we repeated the experiments using pulse-interleaved excitation, which verified that the acceptor remained fluorescently active throughout the entire trajectory (Fig. S7). Given that the dwell time (several ms) is much longer than the timescale of the dynamics of an unfolded protein chain (10's – 100's ns),[29] there is ample time for the chain segment to explore the entire cross-sectional area of the pore at any given point in the translocation process. For the sake of simplicity, we discuss the ε_{calc} values corresponding to a chain located in the center of the lumen (red center line in Fig. 1c). Comparing E_{peak} values (Fig. 2b) to the ε_{calc} map (Fig. 1c), it becomes apparent that the moderate E_{peak} values of ca. 0.5 correspond to instances in which the tagged residue of casein only begins to enter the pore (> 3 nm depth). If entry is via the NTD, it indicates that casein has reached the NBD1 but has not made it past the first set of pore loops (PL1, located at a depth of ca. 3.4 nm). On the other hand, the 45% of E_{peak} values ≥ 0.7 must originate from events where casein reaches deep into the lumen of ClpB, near the interface between the two NBDs. This could be accomplished by casein entering through the NTD ring, reaching NBD1, and passing through (at least) the first two sets of pore loops (PL2 depth is ca. 4.4 nm), corresponding to a translocation depth of at least ca. 5 nm into the lumen.

To examine whether translocation events culminated in a complete passage through the lumen of ClpB, we repositioned the donor molecule to the NBD2 of ClpB (res. 771, Fig. 2a bottom). In this position, high FRET efficiency events can only occur if casein passes through the NBD2 ring (see Fig. S8). The sample trajectory shown in Fig. 2a bottom (in purple) is remarkably similar to those obtained with the NBD1-labeled ClpB (Fig. 2a top). In fact, the 1214 events measured across 137 trajectories displayed a similar power-law distribution (a =1.55 ± 0.02, Fig. 2b), and identical average event time ($<\tau_{dwell}>$ = 1.6 ± 0.1 ms) and E_{peak} values (Fig. 2c) compared to those of the NBD1-labeled protein. A summary of statistics is provided in Tables S1 and S2, and additional sample trajectories for both labeling locations can be found in Figs. S9 and S10. The low E_{peak} values of ca. 0.5 (Fig. 2c) correspond to events where casein has made its way past the first two PL rings but failed to complete translocation across NBD2. However, the high E_{peak} events, constituting 45% of all events, necessitate that the acceptor-labeled segment has completed passage through the NBD2 and through the third ring of pore loops (PL3, depth of ca. 7.8nm). The similar $<\tau_{dwell}>$ values for NBD1- and NBD2-labeled ClpB suggest that the longitudinal motions (estimated to correspond to distances of 8.1 and 6.2 nm, respectively, based on the region in the ε_{calc} maps where ε_{calc} > 0.5), occur rapidly across both NBDs. While these fast events only represent snapshots of motion corresponding to contour lengths of ca. 16 – 20 *aa*'s along casein, the overwhelming frequency of these short events points towards a rapid translocation mechanism spanning both NBDs.

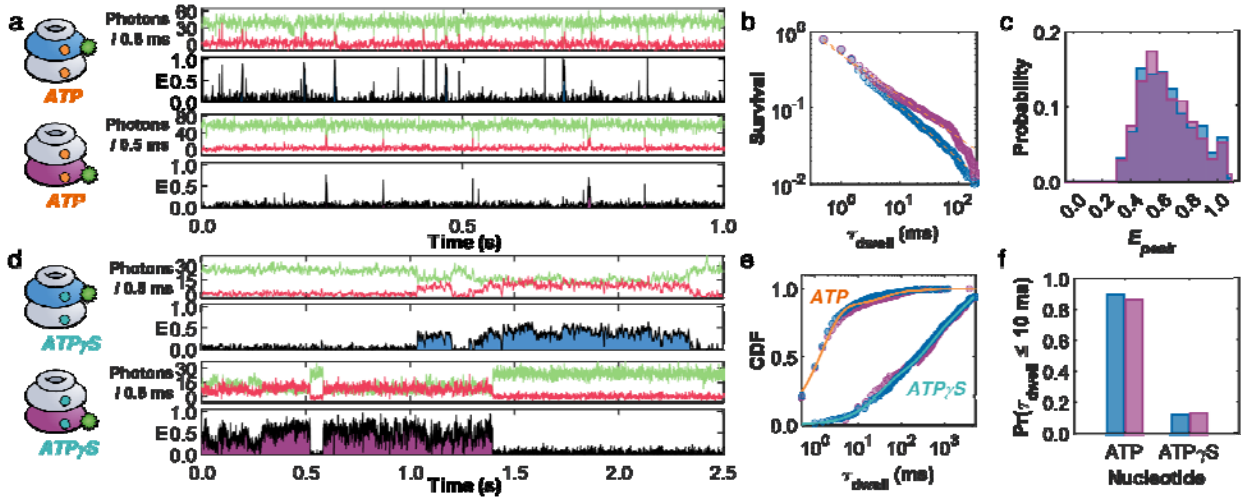

Figure 2. ATP, but not ATPγS, sustains rapid substrate processing. Sample trajectories in the presence of **a,** 2 mM ATP or **d,** 2 mM ATPγS. ClpB was labeled with a donor either on (blue, top trajectory) NBD1 (res. 359C) or (purple, bottom trajectory) NBD2 (res. 771C). **b,** The survival probability of the events for NBD1- (blue) and NBD2- (purple) labeled ClpB are nearly identical, with power-law fits (dashed lines) yielding powers of 1.69 ± 0.02 and 1.55 ± 0.02, respectively. **c,** Histogram of the peak FRET efficiency E_{peak} for the events in b. **e,** Cumulative distribution function (CDF) of the event times for the two labeling locations in the presence of ATP and ATPγS. The solid lines represent triexponential fits of the dwell times in the presence of (orange) ATP and (teal) ATPγS, providing average values of 21.8 ± 0.3 and 749 ± 4 ms, respectively. **f,** The presence of ATPγS suppresses the fraction of short (< 10 ms) events in both labeling locations, demonstrating that the fast translocation events are ATP-dependent.

Millisecond translocation is ATP-dependent. The threading velocity through ClpB (~ 20 *aa*'s in 2 ms) estimated from the above experiments is much faster than expected for AAA+ motors based on their overall ATPase activity and on previous bulk,[30,31] or single-molecule[32] studies, begging the question as to whether the events measured here truly represent ATP-dependent translocation. While it would be tempting to simply remove ATP to abolish ClpB activity, the hexameric assembly of ClpB necessitates the presence of ATP or an analog.[33] The slowly hydrolysable ATPγS (adenosine-5′-o-3-thio-triphosphate) is known to hamper the translocation activity of ClpB, resulting in a *holdase*-like behavior.[34] We, therefore, tested events of interaction between ClpB and casein in the presence of 2 mM ATPγS, collecting 337 events from 147 molecules with the NBD1 labeling location and 227 events from 113 molecules with the NBD2 labeling location. Notably, compared to the same labeling locations in the presence of ATP, there was a > 4-fold reduction in the average number of events (compare to >1200 events for a similar number of molecules with ATP, Table S2). Fig.e 2d provides sample trajectories for both labeling locations on ClpB (NBD1 in blue, NBD2 in purple) in the presence of 2 mM ATPγS (in teal), demonstrating a substantial increase in the substrate dwell time (see also Figs. S11 and S12). A cumulative dwell time histogram of both labeling locations in the presence of ATP and ATPγS is given in Fig. 2e. While the presence of ATP leads to nearly 90% of the events occurring in less than 10 ms (Fig. 2f), ATPγS suppresses these short events, reducing their frequency to < 15%. Fitting the cumulative distribution of dwell times (solid lines in Fig. 2e, Table S3) revealed that

the weighted average overall dwell time increased from 21.8 ± 0.3 to 749 ± 4 ms when the nucleotide was switched from ATP to ATPγS, corresponding to an increase by a factor of ~34.

In support of these findings, the apparent dissociation constants ($K_{D,app}$) of casein in the presence of both nucleotides were determined by fluorescence anisotropy (Fig. S2). A simple bimolecular binding curve revealed that ATPγS decreased $K_{D,app}$ (= 20 ± 10 nM) by a factor of 30 compared to that of ATP (= 600 ± 10 nM). Importantly, these $K_{D,app}$ values do not represent the true dissociation constant due to the active translocation and disengagement by ClpB but rather depend on the interaction times with casein. Therefore, the agreement between the 30-fold increase in dwell time and apparent equilibrium constants supports the conclusion that the events probed in the single-molecule experiments indeed report on the translocation activity of ClpB. Overall, the presence of ATP generates fast translocation events that last only a few milliseconds. Intriguingly, despite these events occurring on a timescale much faster than the bulk ATPase activity, the presence of ATPγS hinders them considerably, suggesting that with this nucleotide substrates are not quickly released by the machine but rather dwell inside for long periods of time.

Translocation times depend weakly on temperature. To glean further insight into the mechanism of translocation, the temperature dependence of the measured events was investigated by repeating the FRET experiments at two additional temperatures, 10 and 32°C (see Methods for more details). At each temperature, over 60 ClpB molecules were sampled, leading to the observation of hundreds (> 500) of events (Table S1). Sample trajectories are provided in Fig. S13. For both labeling locations, the impact of temperature on τ_{dwell} was surprisingly small, leading to similar power laws, E_{peak} histograms, and fraction of short events (Fig. S14, Table S2). In fact, only a slight increase in the $\langle\tau_{dwell}\rangle$ value from 1.4 to 1.7 ms was observed as the temperature decreased from 32 to 10 °C (Table S2). An Arrhenius plot combining data from both labeling locations (Fig. 3a) revealed a very low activation energy for translocation of E_A = 1.87 ± 0.69 k_BT. For comparison, the molecular motors kinesin and actomyosin, which consume ATP to '*walk*' along microtubules, exhibit significantly larger energy barriers of 20 and 40 k_BT, respectively.[35,36] These established *power-stroke* machines exhibit large barriers due to large conformational changes driving the mechanical work,[12,13,37] as would be expected for a stepping hand-over-hand mechanism of ClpB. Instead, the substantially lower activation energy of ClpB demonstrates that it must utilize a different mechanism for translocation, likely a *Brownian ratchet* (see discussion below).[12,38,39]

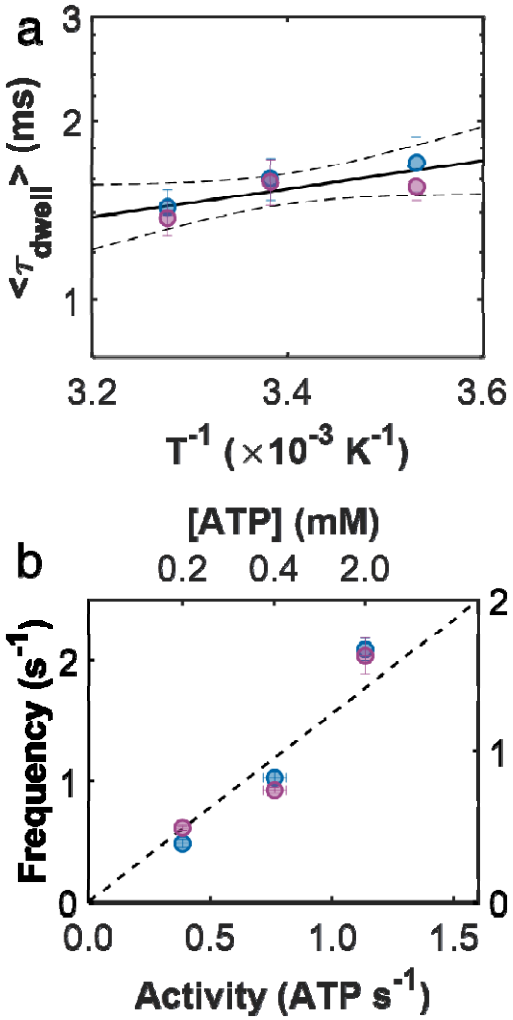

Figure 3. Temperature and ATP concentration dependence measurements support a ratcheting mechanism. a, Arrhenius plot (logarithm of $<\tau_{dwell}>$ vs. the reciprocal of temperature) of the average dwell times for the NBD1- (blue) and NBD2- (purple) labeled ClpB. Linear regression (solid black line) returns an activation energy of 1.87 ± 0.69 k_BT. The 95% confidence intervals are provided as dashed lines. **b,** The frequency of events for NBD1- (blue, left axis) and NBD2- (purple, right axis) labeled ClpB as a function of ATPase activity. The ATPase activity of ClpB (bottom axis, Fig. S5) was controlled by varying the ATP concentration (top axis). Note the non-linear scale in ATP concentration. Linear regressions return 1.65 ± 0.18 and 1.29 ± 0.15 events per hydrolysed ATP based on the bulk ATPase activity.

Event frequency directly correlates with bulk ATPase activity. At a saturating concentration of ATP (2.0 mM, Fig. S5), the bulk casein-stimulated ATPase activity of ClpB is only 1.14 ± 0.03 ATP/s, begging the question of how the slow consumption of ATP is related to the two to three orders of magnitude faster translocation events. To answer this question, we repeated single-molecule experiments under conditions with reduced ATPase activity of ClpB. By lowering the concentrations of ATP from 2.0 to 0.4, and 0.2 mM, the bulk ATPase activity was lowered from 1.14 ± 0.03 to 0.76 ± 0.05 and 0.39 ± 0.03 ATP/s, respectively (Fig. S5). Translocation events

from over 100 individual ClpB molecules were collected at each ATP concentration and labeling location (Table S1), and sample trajectories are shown in Fig. S15. Surprisingly, despite the significant reduction in ATPase activity with decreasing ATP concentration, there were only small changes in dwell time distributions, $<\tau_{dwell}>$ values, power-law exponents, and E_{peak} histograms (Fig. S16, Tables S2 and S4). However, there was a significant reduction in the frequency of events (= # of events / trajectory length) as the ATPase activity decreased. Exponential fits of the event frequency (Fig. S17) revealed that the frequency decreased linearly with decreasing activity (Table S5). As seen in Fig. 3b, both labeling locations exhibited very strong correlations (R = 0.98 and 0.95, respectively) between the event frequency and the bulk ATPase activity. The surprising result that decreasing ATP concentrations strongly affects event frequency and only weakly event dwell time reveals the important result that ATP controls the recruitment of protein substrates by the machine. Earlier studies on hexameric AAA+ machines suggest that ATP widens their lumen,[40,41] perhaps explaining the facilitation of substrate recruitment. From the slopes of the results in Fig. 3b, we find that the average numbers of events per hydrolysed ATP molecule are 1.65 ± 0.18 and 1.29 ± 0.15 for NBD1- and NBD2-labeled ClpB, respectively. The larger-than-unity values may suggest that one hydrolysis event can drive more than one translocation event, though they may also be due to the presence of incomplete/partial translocation events in the analysis, which are difficult to separate from complete translocation (but see below).

Three-color smFRET studies reveal bidirectional translocation. While the two-color FRET experiments demonstrated that casein can rapidly translocate past both NBDs, the question remained if these events represented complete translocation. Further, while previous studies suggest the interaction with substrates seems to start at the *N*-terminus, there is no direct proof that translocation can take place only in this direction. To address these aspects, we designed a three-color FRET experiment whereby a donor (Cy3B) was labeled onto the substrate casein, and two acceptors were positioned on ClpB. Using bioorthogonal labeling techniques to ensure location specificity (see Methods), we labeled residues 176 and 771 of ClpB with AF647 (acceptor 1) and CF680R (acceptor 2), respectively. The positions were chosen to maximize the sensitivity to the motion through the lumen while simultaneously minimizing unwanted energy transfer between the acceptors (Fig. S18). A map of the ε_{calc} in Fig. 4a depicts how the FRET efficiency between the dye on casein and each of the dyes on ClpB is expected to change as a function of position throughout the lumen. Given the relative locations of the dyes, acceptor 1 (orange) contributes more while casein traverses the NTD and NBD1, while energy transfer to the second acceptor (red) becomes dominant as casein passes through NBD2 (see Methods for details on FRET efficiency calculations). We collected 1445 signals of events across 135 ClpB molecules with ATP, and 135 events across 110 molecules with ATPγS. Sample trajectories are provided in Fig. S19. In the presence of ATP, the dwell-time distributions (decaying with a power law of 1.68 ± 0.2), the fraction of short events (91% of the events persisted for less than 10 ms), and E_{peak} (= max(E_{app})) values were all in close agreement with the two-color experiments (Fig. S20, Table S2). As expected, the addition of ATPγS significantly reduced the number of observed events and generated a 20-fold increase in dwell time (Fig. S21). These results demonstrated that the three-color experiments with ATP were sampling the same rapid ATP-dependent translocation events discussed earlier. However, with the addition of the second dye, we now had the ability to dissect the results further, providing unprecedented detail to the picture of translocation.

Remarkably, three-color FRET experiments uncovered six types (I - VI) of translocation events. As shown in Fig. 4, multiple translocation events took place in the expected, *forward* direction (type I, starting at the *N*-terminus and proceeding to the C-terminus). Representative type I events in Fig. 4b, left, (and S22) clearly demonstrate that the FRET events begin with acceptor 1 (orange) and terminate with acceptor 2 (red), indicating that casein has completely passed through ClpB. An exponential fit of the E_{app} dwell time distribution of type I events revealed a $<\tau_{dwell}>$ value of 2.1 ± 0.2 ms (Fig. 4d). While this value was very similar to the $<\tau_{dwell}>$ values found in the two-color experiments, these three-color experiments conclusively demonstrate that complete translocation indeed occurs in such a short timeframe. Given the placement of the two dyes on ClpB, the $<\tau_{dwell}>$ values for translocation correspond to a lateral motion of 11.6 nm (i.e. the distance in Fig. 4a where $\varepsilon_{calc} > 0.5$), which translates into an overall average translocation velocity of 14 *aa*/ms in the *forward* direction. Based on this estimate, the 190 *aa* long casein, corresponding to a contour length of ca. 76 nm, would take only ~14 ms to be fully translocated through the lumen of ClpB. Both bulk stopped-flow mixing experiments[42] and single-molecule optical tweezer assays[16] support of such fast translocation events. While the short range of FRET limits our ability to rule out a combination of translocation steps and pauses, as proposed by single-molecule optical tweezer assays,[16,32,43] the lack of any intermediate FRET efficiency values in our data rather points towards a continuous translocation mechanism. In fact, sustained rapid translocation with speeds greater than 2.8 nm/ms (equivalent to ~ 7 *aa*/ms) has been observed in DNA-translocating AAA+ proteins.[44]

Perhaps not less surprising than the ultrafast forward translocation events was the existence of events that proceeded in the *backward* direction (type II, starting at the *C*-terminus and continuing to the *N*-terminus, Fig. 4b, and Fig. S23). In fact, 25% of all complete translocation events occurred in the *backward* direction, where casein enters ClpB from the NBD2 (generating fluorescence in the second acceptor, marked red) side, diffuses past all three sets of PLs, and exits through the NTD (generating fluorescence in the first acceptor, marked orange). While it has been assumed that translocation occurs only in the *forward* direction up until this point, this study not only reveals the existence of *backward* threading but also demonstrates that they occur in relative abundance, highlighting their significance in the translocation activity of ClpB. These type II events differed from their type I counterparts in that their $<\tau_{dwell}>$ value of 6.6 ± 1.9 ms (Fig. S20) was about three times slower, suggesting a preferential forward bias in diffusion across the pore loops.

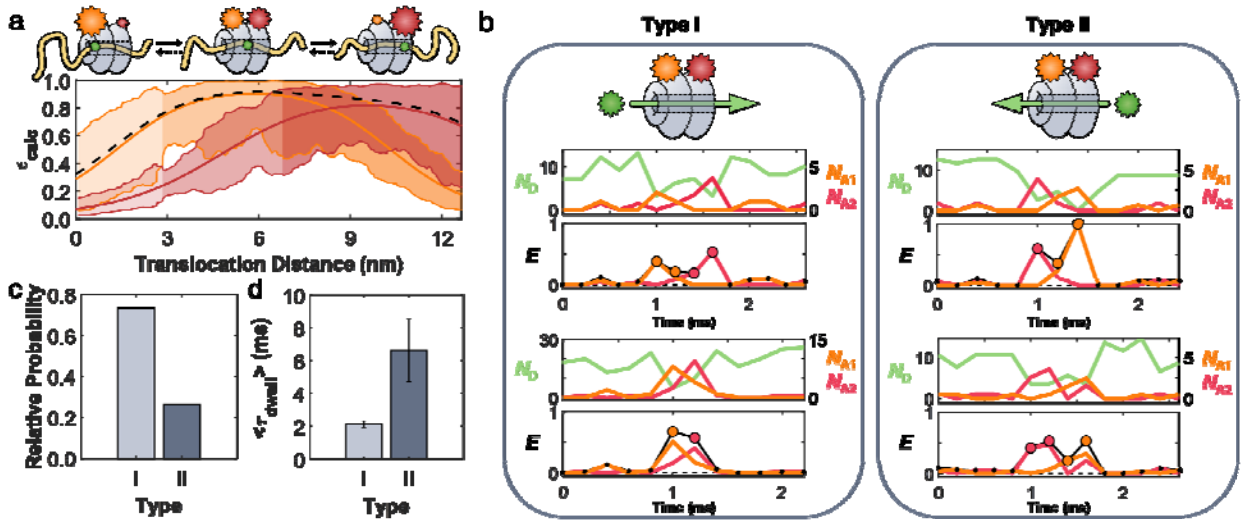

Figure 4. Complete translocation of casein occurs in both the forward and backward directions. a, Map of the calculated FRET efficiency as a function of location throughout the lumen of ClpB with acceptors located on the NBDs of ClpB (acceptor 1: AF647 (R_0 ~ 6.2 nm), orange, res. 176, and acceptor 2: CF680R (R_0 ~ 7.2 nm), red, res. 771). The thick orange, red, and black (dashed) lines represent the calculated FRET efficiency through the center of the pore to acceptors 1 and 2, and the total FRET efficiency, respectively. The shaded areas represent the limits of the FRET efficiencies based on the boundaries of the pore. **b,** Complete translocation events through ClpB. Type I – *forward* translocation events starting at the NTD and exiting past the NBD2. Type II – *backward* translocation events starting at the NBD2 and exiting past the NTD. Samples of the fluorescence of the donor (green, N_D) and acceptors (acceptor 1: orange, N_{A1} and acceptor 2: red, N_{A2}) and apparent FRET efficiency ($E_{A1} = N_{A1} /(N_D + N_{A1} + N_{A2})$, $E_{A2} = N_{A2} /(N_D + N_{A1} + N_{A2})$, and overall apparent efficiency as the black trace $E_{app} = E_{A1} + E_{A2}$) are provided. Each bin was assigned a color based on which acceptor was more prevalent (i.e., which acceptor experienced greater energy transfer from the donor, see Methods) as indicated by the coloring of the data points in the FRET efficiency trace. Additional samples of type I and II events are provided in Figs. S22 and S23. **c,** The fractions of complete translocation events in the *forward* and *backward* directions (when considering only complete translocation events), and **d,** the average event times retrieved from an exponential fit of the dwell time distribution (Fig. S20).

Partial threading events. In addition to complete *forward* and *backward* translocation, the three-color FRET experiments also identified partial translocation events. Types III and IV events in Fig. 5a (also in Fig. S24) correspond to incomplete translocation events where casein reaches deep into the lumen, reaching both NBDs and thus exhibiting energy transfer to both acceptors. However, the signals began and ended with the same acceptor, demonstrating that casein entered and exited from the same side of ClpB. While partial threading events have been inferred from previous studies,[17,45] we directly demonstrate their existence here, also noting that they occur in a bidirectional manner. As in the case of type I and II events, a notable feature is that the *forward* type III events were significantly more abundant than *backward* type IV events (Fig. 5b). However, type III events typically took 11.3 ± 3.1 ms, over 5 times longer than the type I events (Fig. 5c). On the other hand, the *backward* type IV events, with a $<\tau_{dwell}>$ of 6.2 ± 0.5 ms, lasted for nearly identical times as the *backward* type II complete translocation events.

Another interesting feature is that the relatively long dwell times of both type III and IV events appear to originate from rapid back-and-forth motions of casein, as seen in the frequent interconversion between the two acceptors (orange and red) in the sample trajectories given in the top of Fig. 5a. Such a feature suggests that the long dwell times of these events are related to back-and-forth motions of the substrate in the lumen before exiting. In fact, a correlation plot between τ_{dwell} and the number of back-and-forth motions revealed a correlation coefficient of R = 0.982 (Fig. 5d).

Lastly, type V (*forward*) and VI (*backward*) events (Figs. 5a and S25) were attributed to casein superficially binding, but not entering the lumen, resulting in the appearance of energy transfer to only one of the acceptors. Both type V and VI events exhibited very brief dwell times of under 0.5 ms (Fig. 5c), suggesting that these events represent instances where casein attempts to enter the lumen but fails to make it past one of the NBDs (which would result in energy transfer to both acceptors) before dissociation.

Overall, only two-thirds of all events started at the *N*-terminus of ClpB, while the rest started at the *C*-terminus. It is possible that in the presence of ClpB's co-chaperones, such as DnaK and DnaJ that typically required for aggregate recognition, a larger fraction of translocation events would originate from the *N*-terminal side.[4] However, even without these co-chaperones, the NTD binding groove on ClpB is known to bind substrates such as casein,[46] and therefore likely contributes to the observed two-fold increase in probability for events that begin at the *N*-terminus. A complete list of the frequency of each event type and their corresponding dwell times is provided in Table S6.

In the presence of ATPγS, we found that there was a five-fold reduction in the number of events per ClpB molecule, similar to the four-fold reduction in interactions observed in the two-color experiments. Fitting the overall cumulative distributions of dwell times (Fig. S26), it was found that ATPγS increased the overall dwell time by a factor of 20 compared to that of ATP. The lower factor than the one found in the two-color and fluorescence anisotropy experiments (~30) can be attributed to premature photobleaching of the donor before substrate disengagement due to the increased laser power (see Methods). Despite the limited number of 135 events (across 110 ClpB molecules), we nonetheless found that ClpB exhibits all six types of events in the presence of ATPγS. However, the fractions of *forward* and *backward* events were nearly equivalent to each other in all cases, indicating that with ATPγS, the *forward* vs. *backward* bias vanishes. Importantly, this result demonstrates that ATP is necessary to rectify translocation in the *forward* direction. A summary of the frequency of each event alongside their corresponding dwell times can be found in Tables S6 and S7.

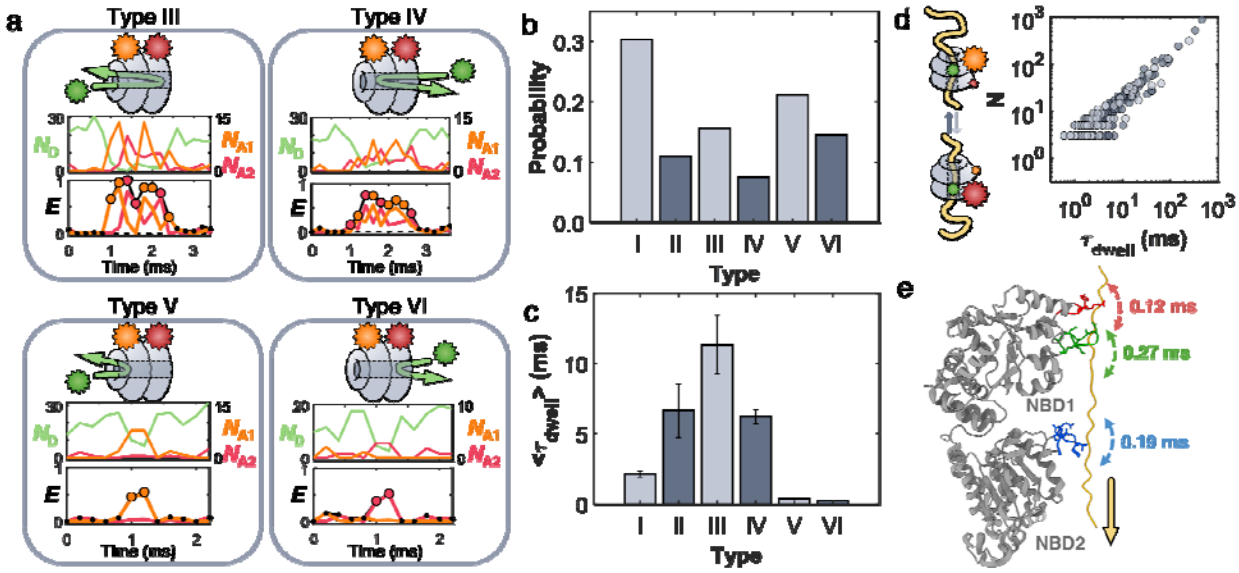

Figure 5. ClpB exhibits partial translocation events. a, Sample incomplete translocation events. Type III (*forward*) and IV (*backward*) partial translocation events are characterized by casein reaching both NBDs but exiting cis to the entry side. Type V (*forward*) and VI (*backward*) fleeting events are characterized by an interaction with only a single NBD. **b,** Probability of occurrence of the different translocation events. **c,** Average event times obtained from the exponential fit of the distribution for each event type (Fig. S20). **d,** Correlation between the number (N) of back-and-forth motions and the dwell times for type III (light) and IV (dark) events. The correlation coefficient of $R = 0.98$ demonstrates that the long dwell times are directly proportional to N. The cartoon inlay illustrates the back-and-forth motions of casein. **e,** Schematic of the previously determined sub-millisecond dynamics of the pore loops (PLs) in the presence of ATP and casein.[18] The three PLs (red, green, and blue) on each subunit directly engage the substrate and rapidly move up-and-down (PDB 6OAX[47]). These fast dynamics modulate the energy landscape between two (or more) rapidly interconverting states. ATP allosterically regulates the dynamics and conformational states of the PLs,[18] generating a landscape in which the substrate preferentially diffuses *forward* from NBD1 to NBD2.

ClpB drives diffusive-like translocation. The translocation activity of ClpB demonstrated in this work is surprisingly rich and very different than expected based on structural studies of AAA+ machines. It is clear from the abolishment of the short events and loss of preferred directionality in the presence of ATPγS that rapid translocation is tightly coupled to ATP. Furthermore, these experiments conclusively demonstrate that ClpB facilitates both partial and complete translocation events in a bidirectional manner, albeit with a preference for *forward* motion. In and of itself, the bidirectional nature of translocation suggests that the energy landscape throughout the translocation process must be shallow. Indeed, the temperature study revealed an activation energy of only ~ 2 k_BT. However, we can gain deeper insight into the landscape by considering the dwell times and frequency of the different types of events.

First, we find that the complete *forward* translocation events are, on average, over five times faster than the incomplete or *backward* translocation events. Based on this ratio, transition state theory suggests that the difference in free energy between the *forward* and *backward* threading directions ($\Delta\Delta G = \Delta G_{forward} - \Delta G_{backward} = -\ln(\langle\tau_{dwell}\rangle_{forward} / \langle\tau_{dwell}\rangle_{backward})$)[48] is no greater than 1 – 2 k_BT. Next, casein was twice as likely to initiate an event at the NTD compared

to the NBD2. Despite this significant preference, the probability for casein to 'enter' into the lumen (quantified by the appearance of FRET to both acceptors, i.e. types I to IV) is only slightly larger when casein approaches via the NTD (Pr('*enter*'|NTD event) = 0.68) compared to that at the NBD2 (Pr('*enter*'|NBD2 event) = 0.56). This suggests that the free-energy contribution of the preferential NTD binding is minor. The barrier for entry, therefore, must be dominated by another factor, such as the loss of chain entropy of casein as it enters the pore, which is expected to be on the order of ~ 9 k_BT.[49] Lastly, considering the scenario where casein has entered the lumen (i.e. not including the superficial types V and VI events), we find that casein is only slightly more likely to exit past NBD2 (Pr('*exit via NBD2'*) = 0.59, types I and IV) than past the NTD (Pr('*exit via NTD'*) = 0.41, types II and III). The Curtin–Hammett principle[50] suggests that the difference in transition-state energies ($\Delta\Delta G^{\ddagger}$ = –ln(Pr('*exit via NBD2*')/Pr('*exit via NTD*')) between the *forward* and *backward* directions is less than 1 k_BT.

Our experiments paint a picture of a shallow landscape where, at any given time, casein is nearly as likely to diffuse in either direction. Further evidence for diffusive-like translocation arises from the type III and IV events, which exhibit hallmarks of rapid back-and-forth motions of casein within the lumen and show a direct correspondence between the number of these motions and the duration of the events. Notably, we observe that diffusion must occur quickly, resulting in translocation within just a few milliseconds. Remarkably, limiting the supply of ATP did not significantly alter the translocation time but rather reduced the frequency of translocation events, indicating that ATP must regulate substrate recruitment in addition to translocation directionality and speed. Moreover, we find that there are, on average, ~ 1.5 events per hydrolysed ATP. Based on the 41% probability of complete threading, we calculate that each complete threading event correlates with the consumption of only 1.65 ± 0.29 ATP molecules. Together, these features suggest a mechanism where the utilization of just one or two ATP molecules is sufficient to drive rapid bidirectional translocation events. It is important to note that while Hsp100 activity may involve both releasing a protein from an aggregate and the subsequent translocation through the central pore, potentially requiring distinct mechanisms of action,[1,42] our experiments with the intrinsically disordered casein focus on the latter and represent the translocation process in the absence of any potential rate limitation due to the disaggregation step.

ClpB as a Brownian motor. Two mechanisms have been proposed for translocation: the *power-stroke* and the *Brownian motor*.[12,13,39,51,52] While they can share some nuanced characteristics,[51] they are classically quite different from one another. The power-stroke mechanism involves significant, fuel-driven conformational changes that generate irreversible translocation steps along a downhill free energy landscape. In contrast, the *Brownian motor* does not depend on large, coordinated motions. Instead, substrate movement is driven by thermal noise (Brownian motion), while an external energy source introduces some form of asymmetrical changes within the free energy landscape. This asymmetry restricts diffusion to one direction, resulting in directed motion.

The features of the mechanism utilized by ClpB discussed above are consistent with those of a *Brownian motor*,[12,39] and are not commensurate with a fully coupled *power-stroke-like* operation. In fact, the rapid translocation by ClpB is more akin to findings on transmembrane pores (e.g., α-hemolysin[53] and Cytotoxin-K,[54] both with a similar 2 nm pore diameter to ClpB), though in these cases, electric potential differences drive biomacromolecules across a membrane. But the question remains, how does ClpB utilize the energy from ATP to drive directional

translocation? From our earlier studies,[18,55] we know that the substrate-engaging pore loops (PLs) lining the lumen of ClpB exhibit sub-millisecond up-and-down motions (Fig. 5e). Importantly, these stochastic ultrafast PL dynamics persist under all nucleotide conditions and even in the presence of casein. However, the populations of their conformational states are allosterically regulated, leading to nucleotide-dependent asymmetries in the orientations of the PLs.[18] Within this framework, we propose a ratcheting mechanism in which the substrate encounters an energy landscape with a preferred direction generated by PL dynamics. The rapid and asymmetric interconversion between PL states facilitates the rapid motion of casein within the lumen while rectifying translocation in the *forward* direction. This driven motion of the substrate occurs on a timescale much faster than that of ATP hydrolysis. Therefore, it stands to follow that the consumption of one (or two) ATP is likely sufficient to generate many ratcheting motions, supporting the above result that complete translocation requires only one or two ATP molecules.

To explore whether the previously observed sub-millisecond dynamics of the PLs correlate with the millisecond translocation events observed in this study, we calculated the average time and amplitude for each of the three sets of pore loops to complete their up-and-down motions in the lumen (Table S8). As depicted in Fig. 5e, PLs 1, 2, and 3 take an average time of 0.12, 0.27, and 0.19 ms, respectively,[18] to complete one up-and-down lateral motion of 1.4 – 1.7 nm.[55] By multiplying the time to complete one up-and-down 'cycle' by the amplitude of motion, we find that the PL dynamics correspond to motions of 16 – 28 *aa*/ms (for PL2, (1.7 nm amplitude of motion) × (1 *aa* / 0.4 nm) / (0.27 ms per 'cycle')). These fast motions represent the expected limiting speed for a substrate traversing the rapidly evolving PLs and closely align with the ~ 10 *aa*/ms velocity estimated from the 2-color experiments, as well as the 14 *aa*/ms velocity found for the type I events. While the PLs remain dynamic in the presence of ATPγS, they lose their asymmetry,[18] thereby abolishing the asymmetric landscape required for rapid directional translocation. Lastly, simulations demonstrate that rapid motions of asymmetrical restrictions in a pore, such as the up-and-down movements of the PLs, produce directional translocation as a result of entropic forces,[56,57] supporting our model. It is noteworthy that entropically driven translocation is weakly dependent on temperature,[58] further agreeing with our findings.

Conclusions. In conclusion, this study demonstrates that the translocation of the substrate casein through the AAA+ machine ClpB takes only milliseconds. ATP is essential for these rapid translocation events, and a limited supply of ATP reduces event frequency but not velocity, underscoring its role in substrate recruitment. Crucially, we reveal that translocation operates bidirectionally, with a 3:1 preference for *forward* threading. Substituting ATP with ATPγS abolishes directionality and hinders translocation, reinforcing the essential role of ATP. However, translocation is not driven by power strokes following ATP hydrolysis events. The observed diffusive-like behavior and low energy barriers associated with bidirectional motion strongly support a *Brownian motor* mechanism for ClpB and AAA+ proteins in general, where ATP guides activity and directionality but does not directly generate force steps. *Brownian motors* use an energy source to rectify diffusive motion[12] and have been broadly studied as physical models for dissipative dynamics.[59] A direct observation of such motors in the context of biological nanomachines remains rare. More broadly, this work has implications for other biomolecular machines that couple ATP hydrolysis to substrate translocation, including protein disaggregases, unfoldases, and translocases across diverse cellular systems.

Methods and Materials

Protein expression and purification: *Thermus thermophilus* ClpB with a six-residue histidine tag at its *C*-terminus was cloned into a pET28b vector. All ClpB mutants were generated by site-directed mutagenesis and standard cloning techniques and were verified by DNA sequencing. The wild-type (WT) and single mutant ClpB proteins (359C and 771C) were expressed and purified as previously reported.[27] A double-mutant ClpB incorporated the unnatural amino acid *N*-ε-(prop-2-ynyloxycarbonyl)-*L*-lysine (ProK, Iris Biotech) at residue 771, and a cysteine at residue 176. ProK was coded with the Amber stop codon, allowing for co-transfection of the double mutant 176C + 771TAG ClpB in pET28b together with pEvol PylRS/tRNApyl[60] (Addgene, Plasmid #127411, back mutated to A346N/A348C) into *E. Coli* BL21 (DE3) pLysS cells (Invitrogen) using heat shock. Cells were recovered and incubated in 10 mL Luria Broth (LB, Thermo Fisher) media containing kanamycin (Sigma, 50 μg/mL) and chloramphenicol (Sigma, 25 μg/mL) for 16 h at 37 ºC, 250 rpm. The overnight culture was used to inoculate 1 L of LB supplemented with corresponding antibiotics and arabinose (Formedium, 0.2 w/v%). After reaching an optical density (OD) of 0.5, the temperature was reduced to 25°C, and ProK (2 mM) was added. After reaching an OD of 0.8, ClpB expression was induced by the addition of isopropyl ß-D-1-thiogalactopyranoside (Sigma, 1 mM) and incubated for 24 hours. Purification was conducted in a similar manner as above. Briefly, cells were harvested and lysed using a French press, followed by heat shock treatment (80°C, 10 min.). ClpB was recovered from the supernatant on a Ni Sepharose column (HisTrap FF, Cytiva), and dialyzed (50 kDa molecular weight cutoff, Gene Bio-Application Ltd.) overnight.

Protein labeling and subunit mixing: Single-mutant ClpB was labeled with cyanine 3B maleimide (Cy3B, Cytiva) following a previously reported procedure.[27] κ-casein (Sigma) was labeled in a similar manner with either Cy3B or the cyanine-based dye 660R maleimide (CF660R, Biotium). The probability of labeling casein (containing two native cysteines) with two dyes was minimized by reducing the dye ratio to 0.6 eq. per protein molecule (see *distribution of labeled casein inside liposomes* in the SI for more details). Excess dye was removed using a desalting column (Sephadex G25 Superfine, Cytiva), followed by overnight dialysis (8 kDa, Gene Bio-Application Ltd.) against HEPES buffer (25 mM HEPES (J.T. Baker), 25 mM KCl (Sigma), 10 mM $MgCl_2$ (Sigma), pH 8). The ClpB double mutant was first labeled with Alexa Fluor 647 maleimide (AF647, Thermo Fisher), after which the unnatural amino acid was reacted with CF680R azide (Biotium) through copper-mediated click chemistry. Briefly, CF680R (4 eq.) was added to a solution of AF647 labeled ClpB (500 μL, 13 μM) in phosphate buffer (Sigma, 100 mM, pH 7). Next, $CuSO_4$ (Sigma, 200 μM) and tris-hydroxypropyltriazolylmethylamine (Lumiprobe, 1 mM) were added. The labeling reaction was then initiated with the addition of sodium ascorbate (Sigma, 5 mM) and the protein was left to react for 2 hours. Afterwards, the reaction was quenched by the addition of ethylenediaminetetraacetic acid (EDTA, 2 mM). ClpB was separated from the reaction mixture using a desalting column (HiTrap, Cytiva). Any remaining copper or small molecules were removed by overnight dialysis (50 kDa) against a HEPES buffer containing EDTA (2 mM).

Hexameric assemblies of ClpB containing at most one single fluorescently labeled subunit were prepared by reassembling a mixture of labeled ClpB (1 eq.) with an excess (20 eq.) of wild-type ClpB. Homogeneous mixing of the subunits was ensured by performing the procedure in the presence of the guanidinium chloride (GdmCl, 6M, Sigma) overnight. The denaturant was slowly removed by repeated dialysis (50 kDa) against HEPES buffers containing

4, 2, 1, 0.5, and 0 M GdmCl in four-hour intervals. The reassembled subunits were then dialyzed further against a HEPES buffer containing ATP (Sigma, 2 mM). The samples were then filtered (0.1μm, Whatman Anotop), aliquoted, flash-frozen, and stored at –80°C until further use. The low salt of the HEPES buffer (25 mM HEPES, 25 mM KCl, 10 mM $MgCl_2$, pH 8) and the persistence of nucleotide after reassembly ensured that ClpB remained in a hexameric assembly in all experiments.[27,61,62] Native gel demonstrating the reassembled ClpB is provided in Fig. S5. The rotational freedom of the covalently bound dyes are quantified in the *fluorescence anisotropy decay experiments* section in the SI.

ATPase Activity: The ATPase activity of ClpB was measured according to a previously published procedure[27] using a coupled colorimetric assay.[63] Briefly, ClpB (ca. 1 μM) was incubated in a buffer (25 mM HEPES, 25 mM KCl, 0.01% tween-20, pH 8) with an enzymatic ATP regeneration system (2.5 mM phospheonol pyruvate (Sigma), 10 units/mL pyruvate kinase and 15 units/mL lactate dehydrogenase (from rabbit, Sigma)), to which were added 1,4-dithioerythritol (2 mM, Sigma), EDTA (2 mM), nicotinamide-adenine dinucleotide (NADH, reduced form, 0.25 mM), and ATP (varied from 0 to 2 mM) at 25°C. The reaction was started by the addition of $MgCl_2$ (12 mM). ATP hydrolysis was measured by monitoring the decrease of NADH absorption (340 nm) in time on a microplate reader (CLARIOstar, BMG Labtech). The ATPase activity of ClpB in the presence of casein (3 μM) and in its absence is shown in Fig. S5.

Surface-tethered lipid vesicle preparation: Following a previously published procedure,[64] the fluorescently labeled protein molecules were encapsulated inside unilamellar vesicles, which were subsequently immobilized on a glass-supported lipid bilayer through a biotin-streptavidin linkage. Briefly, vesicles used for the formation of a glass-supported lipid bilayer were prepared from a lyophilized mixture (5 mg) of egg-phosphatidylcholine (Avanti) and 0.2 mol% 1,2-dioleoyl-sn-glycero-3-phosphoethanolamine-*N*-(biotinyl) (18:1 biotinyl PE, Avanti), which was reconstituted into a HEPES buffer (1 mL) by mixing. The suspension was extruded 75 times through a 0.1 μm filter (Whatman Anotop) to form unilamellar vesicles. The vesicle solution was inserted into a glass flow cell for 15 minutes, then rinsed with HEPES buffer, leaving behind a supported lipid bilayer on the interior surfaces of the cell. The cell was flushed with a solution of streptavidin (1 mg/mL), which attached to the biotinylated lipids. Vesicles containing ClpB and casein were prepared by reconstituting a lyophilized mixture (3 mg) of 1% mol biotinyl PE in 1,2-dimyristoyl-sn-glycero-3-phosphocholine (DMPC, Avanti) with a HEPES buffer solution containing ATP (2 mM), ClpB (200 nM), casein (3 μM), ascorbic acid (AA, 2 mM, Sigma) and protocatechuic acid (PCA, 1.5 mM, Sigma). The mixture was then extruded 75 times through a 0.1 μm filter to generate unilamellar vesicles with a ca. 120 nm diameter. Unencapsulated casein was removed by passing the liposome mixture through a MicroSpin S-400 HR column (Cytiva). Importantly, while the initial sample contained a 150-fold excess of casein, this ratio was carefully chosen so that the resulting liposomes would only contain a single molecule of casein and be sparsely populated with ClpB, leading to a near 1:1 ratio between the proteins in the ClpB-containing liposomes. The vesicle solution was diluted (1:100) and incubated inside the lipid-bilayer coated flow cell for 5 minutes to allow binding to the immobilized streptavidin. Unbound vesicles were removed by washing (3 x 200 μL) with the HEPES buffer containing ATP (2 mM, adjusted for experiments conducted at different concentrations). The HEPES buffer (100 μL, outgassed with N_2 to remove oxygen) with the addition of an oxygen-scavenging system[65,66] (1.5 mM PCA and ca. 5 nM protocatechuate 3,4-dioxygenase), a triplet quenching

and radical scavenging system[66,67] (2 mM AA, 1 mM methyl viologen) and ATP (2 mM, adjusted for experiments conducted at different concentrations) was added to the flow cell before sealing with silicone grease. Experiments in the presence of ATPγS (Roche, 2 mM) were prepared in a similar manner but were left to incubate with ATPγS for 40 minutes before reconstitution into liposomes.

smFRET data acquisition: Single-molecule fluorescence data were acquired using a PicoQuant Microtime 200 confocal microscope. Two-color measurements were conducted in a continuous wave mode using a circularly polarized 561 nm laser with a power of ca. 400 nW (polarization was measured at the objective (Olympus, UPlanFLN 100X/1.30 Oil Iris)). The positions of liposomes containing fluorescently labeled species were identified by raster scanning a piezo-driven stage (Physik Instrument, P-721.CLQ and P-733.2CL), and the fluorescence of individual liposomes was monitored until photobleaching of the donor dye. The instrument was equipped with a ZT405/488/561/640rpcv2 (Chroma) primary dichroic mirror, the emission was split between the donor (Cy3B) and acceptor (CF660R) channels using a T635lpxr dichroic mirror (Chroma) and filtered using a 593/46 Brightline (Semrock) or a 731/137 Brightline bandpass filter (Semrock).

To increase the time resolution for the three-color experiments, we elected to perform the experiments under increased laser power (from 400 to 700 nW), which nevertheless still allowed obtaining fluorescence trajectories of a reasonable length. Three-color experiments were conducted using 40 MHz pulsed lasers with a sequence of one pulse of the acceptor laser (640 nm, ca. 50 nW) followed by three pulses of the donor laser (530 nm, ca. 700 nW). The excitation was circularly polarized, as measured at the objective. The positions of liposomes containing labeled ClpB were identified using an acceptor-only raster scan with a power of ca. 500 nW. The instrument was equipped with a TZ532/640rpc primary dichroic mirror (Chroma), and the emission was split into donor and acceptor by a T635lpxr dichroic mirror (Chroma). The acceptor emission was further split by a T685lpxr dichroic mirror (Chroma) into two acceptor channels (AF647 and CF680R). Before reaching the detector, the donor emission was filtered with a 582/75 Brightline bandpass filter (Semrock). The acceptor channels were filtered with a ET667/30m or a ET720/60m bandpass filter (Chroma) for the AF647 and CF680R channels, respectively.

smFRET data analysis: The apparent FRET efficiency ($E_{app} = N_A / (N_D + N_A)$) of the two-color experiments was calculated using the photon counts (binned to 0.5 ms) from the acceptor (N_A) and donor (N_D) after corrections for background photons and channel crosstalk (i.e. acceptor emission detected in the donor channel and donor emission detected in the acceptor channel). Background flux was determined by the residual photon count in each channel after photobleaching of the donor, and channel crosstalk was found from trajectories of isolated donor- and acceptor-labeled molecules within liposomes. The acceptor had negligible crosstalk, while the donor had 13% of its emission appear in the acceptor channel. Further discussion on channel crosstalk can be found in the *derivation of leak and background corrections* and the *leak-factor determination* sections of the SI. Translocation events in the trajectories were identified by peaks in the E_{app} trajectories where E_{app} exceeded 0.3. Since this method did not account for the rising and falling edges of the events, the edges were extended until the E_{app} value was no longer statistically different (1.5 σ) than the local background values (using a sliding window of 7 bins).

The dwell time τ_{dwell} of each event was taken as the length of each agglomerated region. E_{peak} values were taken as the maximum E_{app} value from the identified events.

While an explicit calculation of bona fide FRET efficiency values in multicolor experiments can be performed,[68] for the purpose of this work, we elected to calculate apparent FRET efficiencies in simpler terms, directly using the experimentally obtained photon count rates of the donor (N_D) and the two acceptors (N_{A1} and N_{A2}).[68,69] The apparent FRET efficiencies in three-color experiments were calculated using the photon counts from 0.2 ms bins after background correction. Due to the relatively low photon counts (~ 10 – 30 photons / bin), applying additional correction factors such as channel crosstalk to the individual trajectories introduced a large amount of unwanted noise and, therefore, was avoided. Further discussion on the correction factors, including inter-acceptor energy transfer, can be found in the *leak-factor determination* and the *determining inter-acceptor energy transfer* sections of the SI. The apparent E_{app} to each acceptor was calculated as $E_{Ai} = N_{Ai} / (N_D + N_{A1} + N_{A2})$, where Ai represents acceptor 1 or 2, and the total apparent FRET as $E_{app} = (N_{A1} + N_{A2}) / (N_D + N_{A1} + N_{A2})$. Following a similar procedure as in the two-color analysis, interaction events were identified using the total E_{app} values, such that the extracted τ_{dwell} values represent the total observed dwell time regardless of which acceptor is more prominent. Once identified, each bin in an event was then assigned a color based on which acceptor was most prominent. While we elected not to apply spectral crosstalk corrections directly to the trajectories, acceptor 1 (AF647) had a moderately large fraction of its emission (37%) appear in the acceptor 2 channel (CF680R). As such, a bin was assigned to acceptor 2 if E_{A2} contributed over 60% of the total E_{app}; otherwise, it was assigned to acceptor 1. The $E_{A2}/E_{app} > 0.6$ cut-off value was chosen because it corresponds to the situation where the donor is experiencing equivalent energy transfer to both acceptors (i.e., after correction for crosstalk, $\varepsilon_{A1} \sim \varepsilon_{A2}$).

Event dwell-time characterization: The length of each event was characterized by the value τ_{dwell} as discussed in the *smFRET data analysis* section. To determine the exponent α of the power law distribution of τ_{dwell} values, $P(\tau_{dwell}) \sim \tau_{dwell}^{-a}$, the survival probability that τ_{dwell} has a value greater than τ, S(τ), was calculated for each point in the distribution, and eq. 1 was fitted to the resulting data.[28] In this equation, P is the probability distribution of τ_{dwell} values, C is a normalization constant, and α is the power for τ_{dwell} values obeying the power law.[28]

$$S(\tau) = \int_{\tau}^{\infty} P(t)\,dt = \tfrac{C}{\alpha-1}\tau^{-(\alpha-1)} \qquad (1)$$

Distributions obeying power laws with α values less than two, as those reported herein, have a divergent mean and variance. Therefore, a representative overall average event time based on the collected statistics was found from the triexponential fit of the cumulative distribution (CDF, eq. 2) of τ_{dwell} values.

$$CDF(\tau) = \int_{-\infty}^{\tau} P(t)\,dt \qquad (2)$$

In the presence of ATP, the short dwell times, representing the vast majority of events (see Table S2), were characterized by an exponential fit of all events occurring in less than 10 ms. In doing so we noted that the few very long interactions did not spuriously skew the average dwell time reflecting the bulk of the short translocation events. Model parameters (and their corresponding standard errors) were optimized with the 'fitnlm' function in Matlab utilizing the Levenberg-Marquardt nonlinear least squares algorithm.

Temperature-dependent smFRET experiments: In these experiments, the temperature inside the fluorescence cell was controlled by equipping the confocal microscope with a custom-built Peltier temperature unit, consisting of four Peltier elements controlling the temperature of an aluminum housing surrounding the cell, and another Peltier element controlling the temperature of an aluminum block directly coupled to the objective. The temperature inside the confocal volume was determined by measuring the change in the diffusion coefficient of Cy3B using fluorescence correlation spectroscopy (FCS). Further information can be found in the *fluorescence correlation spectroscopy* section and Fig. S27 in the SI. The constituents of the vesicular membranes were changed to lipids with transition temperatures close to those of the experiments (18:0 – 18:1 PC and 15:0 PC with transition temperatures of 6 and 35°C, respectively), ensuring the membranes remained permeable to ATP (Figs. S28 and S29). Linear regressions and standard errors were computed using the method of ordinary least squares with the 'fitlm' function in Matlab.

Acknowledgements. We thank Drs. Pierre Goloubinoff, Hagen Hofmann, Axel Mogk and David Scheerer for reading and commenting on the manuscript. This work was supported by a grant from the NSF-BSF program (no. 2021700). Remi Casier is grateful to the Azrieli Foundation for their generous funding of an Azrieli International Postdoctoral Fellowship. We thank Drs. Hagen Hofmann and Tanya Lasitza-Male for the setup and use of their homebuilt Peltier control unit, and Dr. David Scheerer for the fluorescently labeled enzyme adenylate kinase.

Author contributions. R.C., I.R., and G.H. conceptualized and designed the experiments. R.C. conducted the experiments. R.C., D.L., I.R., and B.Y. worked on protein expression, purification, and labeling. R.C. and G.H. analyzed the results and wrote the manuscript. All authors contributed to editing and discussions.

Competing interests. The authors declare no competing interests.

Supplementary Information. Supplementary Information is available for this paper; additional methods section, supporting Figures S1 – S32, Tables S1 – S14, and supporting references.

Data availability. A summary of the data in this manuscript is provided in the Supplementary Information. Additional data supporting the findings of this manuscript are available from the corresponding author upon request.

Correspondence. Correspondence and requests for materials should be addressed to G.H.

References

1 Lin, J., Shorter, J. & Lucius, A. L. AAA+ proteins: one motor, multiple ways to work. *Biochemical Society Transactions* **50**, 895-906 (2022). https://doi.org:10.1042/bst20200350

2 Gates, S. N. & Martin, A. Stairway to translocation: AAA plus motor structures reveal the mechanisms of ATP-dependent substrate translocation. *Protein Science* **29**, 407-419 (2020).

3 Erzberger, J. P. & Berger, J. M. Evolutionary relationships and structural mechanisms of AAA+ proteins. *Annu Rev Biophys Biomol Struct* **35**, 93-114 (2006). https://doi.org:10.1146/annurev.biophys.35.040405.101933

4 Deville, C. *et al.* Structural pathway of regulated substrate transfer and threading through an Hsp100 disaggregase. *Science Advances* **3**, e1701726 (2017). https://doi.org:doi:10.1126/sciadv.1701726

5 Deville, C., Franke, K., Mogk, A., Bukau, B. & Saibil, H. R. Two-Step Activation Mechanism of the ClpB Disaggregase for Sequential Substrate Threading by the Main ATPase Motor. *Cell Reports* **27**, 3433-3446.e3434 (2019). https://doi.org:https://doi.org/10.1016/j.celrep.2019.05.075

6 Yu, H. *et al.* ATP hydrolysis-coupled peptide translocation mechanism of Mycobacterium tuberculosis ClpB. *Proceedings of the National Academy of Sciences* **115**, E9560-E9569 (2018). https://doi.org:10.1073/pnas.1810648115

7 Uchihashi, T. *et al.* Dynamic structural states of ClpB involved in its disaggregation function. *Nature Communications* **9**, 2147 (2018). https://doi.org:10.1038/s41467-018-04587-w

8 Puchades, C., Sandate, C. R. & Lander, G. C. The molecular principles governing the activity and functional diversity of AAA+ proteins. *Nature reviews. Molecular cell biology* **21**, 43-58 (2020). https://doi.org:10.1038/s41580-019-0183-6

9 de la Pena, A. H., Goodall, E. A., Gates, S. N., Lander, G. C. & Martin, A. Substrate-engaged 26S proteasome structures reveal mechanisms for ATP-hydrolysis-driven translocation. *Science* **362** (2018). https://doi.org:10.1126/science.aav0725

10 Puchades, C. *et al.* Structure of the mitochondrial inner membrane AAA+ protease YME1 gives insight into substrate processing. *Science* **358** (2017). https://doi.org:10.1126/science.aao0464

11 Gates, S. N. *et al.* Ratchet-like polypeptide translocation mechanism of the AAA+ disaggregase Hsp104. *Science* **357**, 273-279 (2017). https://doi.org:10.1126/science.aan1052

12 Hwang, W. & Karplus, M. Structural basis for power stroke vs. Brownian ratchet mechanisms of motor proteins. *Proceedings of the National Academy of Sciences* **116**, 19777-19785 (2019). https://doi.org:10.1073/pnas.1818589116

13 Wagoner, J. A. & Dill, K. A. Molecular Motors: Power Strokes Outperform Brownian Ratchets. *J Phys Chem B* **120**, 6327-6336 (2016). https://doi.org:10.1021/acs.jpcb.6b02776

14 Yamasaki, T., Oohata, Y., Nakamura, T. & Watanabe, Y. H. Analysis of the cooperative ATPase cycle of the AAA+ chaperone ClpB from Thermus thermophilus by using ordered heterohexamers with an alternating subunit

arrangement. *J Biol Chem* **290**, 9789-9800 (2015). https://doi.org:10.1074/jbc.M114.617696

15 Iosefson, O., Olivares, A. O., Baker, T. A. & Sauer, R. T. Dissection of Axial-Pore Loop Function during Unfolding and Translocation by a AAA+ Proteolytic Machine. *Cell Rep* **12**, 1032-1041 (2015). https://doi.org:10.1016/j.celrep.2015.07.007

16 Avellaneda, M. J. *et al.* Processive extrusion of polypeptide loops by a Hsp100 disaggregase. *Nature* **578**, 317-320 (2020). https://doi.org:10.1038/s41586-020-1964-y

17 Haslberger, T. *et al.* Protein disaggregation by the AAA plus chaperone ClpB involves partial threading of looped polypeptide segments. *Nature Structural & Molecular Biology* **15**, 641-650 (2008). https://doi.org:10.1038/nsmb.1425

18 Mazal, H., Iljina, M., Riven, I. & Haran, G. Ultrafast pore-loop dynamics in a AAA+ machine point to a Brownian-ratchet mechanism for protein translocation. *Science Advances* **7**, eabg4674 (2021). https://doi.org:doi:10.1126/sciadv.abg4674

19 Doyle, S. M., Genest, O. & Wickner, S. Protein rescue from aggregates by powerful molecular chaperone machines. *Nature reviews. Molecular cell biology* **14**, 617-629 (2013). https://doi.org:10.1038/nrm3660

20 Duran, E. C., Weaver, C. L. & Lucius, A. L. Comparative Analysis of the Structure and Function of AAA+ Motors ClpA, ClpB, and Hsp104: Common Threads and Disparate Functions. *Front Mol Biosci* **4**, 54 (2017). https://doi.org:10.3389/fmolb.2017.00054

21 Sawyer, L. & Holt, C. The Secondary Structure of Milk Proteins and their Biological Function. *Journal of Dairy Science* **76**, 3062-3078 (1993). https://doi.org:https://doi.org/10.3168/jds.S0022-0302(93)77646-8

22 Mirdha, L. & Chakraborty, H. Characterization of structural conformers of κ-casein utilizing fluorescence spectroscopy. *International Journal of Biological Macromolecules* **131**, 89-96 (2019). https://doi.org:https://doi.org/10.1016/j.ijbiomac.2019.03.040

23 Benítez, J. J. *et al.* Probing Transient Copper Chaperone−Wilson Disease Protein Interactions at the Single-Molecule Level with Nanovesicle Trapping. *Journal of the American Chemical Society* **130**, 2446-2447 (2008). https://doi.org:10.1021/ja7107867

24 Cisse, I., Okumus, B., Joo, C. & Ha, T. Fueling protein–DNA interactions inside porous nanocontainers. *Proceedings of the National Academy of Sciences* **104**, 12646-12650 (2007). https://doi.org:10.1073/pnas.0610673104

25 Monnard, P.-A. & Deamer, D. W. Nutrient Uptake by Protocells: A Liposome Model System. *Origins of life and evolution of the biosphere* **31**, 147-155 (2001). https://doi.org:10.1023/A:1006769503968

26 Ainavarapu, S. R. K. *et al.* Contour Length and Refolding Rate of a Small Protein Controlled by Engineered Disulfide Bonds. *Biophysical Journal* **92**, 225-233 (2007). https://doi.org:10.1529/biophysj.106.091561

27 Mazal, H. *et al.* Tunable microsecond dynamics of an allosteric switch regulate the activity of a AAA+ disaggregation machine. *Nature Communications* **10**, 1438 (2019). https://doi.org:10.1038/s41467-019-09474-6

28 Newman, M. Power laws, Pareto distributions and Zipf's law. *Contemporary Physics* **46**, 323-351 (2005). https://doi.org:10.1080/00107510500052444
29 Soranno, A. *et al.* Quantifying internal friction in unfolded and intrinsically disordered proteins with single-molecule spectroscopy. *Proceedings of the National Academy of Sciences* **109**, 17800-17806 (2012). https://doi.org:10.1073/pnas.1117368109
30 Nakazaki, Y. & Watanabe, Y. H. ClpB chaperone passively threads soluble denatured proteins through its central pore. *Genes to Cells* **19**, 891-900 (2014). https://doi.org:10.1111/gtc.12188
31 Rajendar, B. & Lucius, A. L. Molecular Mechanism of Polypeptide Translocation Catalyzed by the Escherichia coli ClpA Protein Translocase. *Journal of Molecular Biology* **399**, 665-679 (2010). https://doi.org:https://doi.org/10.1016/j.jmb.2010.03.061
32 Kotamarthi, H. C., Sauer, R. T. & Baker, T. A. The Non-dominant AAA+ Ring in the ClpAP Protease Functions as an Anti-stalling Motor to Accelerate Protein Unfolding and Translocation. *Cell Reports* **30**, 2644-2654.e2643 (2020). https://doi.org:https://doi.org/10.1016/j.celrep.2020.01.110
33 Zolkiewski, M., Kessel, M., Ginsburg, A. & Maurizi, M. R. Nucleotide-dependent oligomerization of C1pB from Escherichia coli. *Protein Science* **8**, 1899-1903 (1999). https://doi.org:https://doi.org/10.1110/ps.8.9.1899
34 Doyle, S. M. *et al.* Asymmetric deceleration of ClpB or Hsp104 ATPase activity unleashes protein-remodeling activity. *Nature Structural & Molecular Biology* **14**, 114-122 (2007). https://doi.org:10.1038/nsmb1198
35 Kawaguchi, K. & Ishiwata, S. I. Thermal activation of single kinesin molecules with temperature pulse microscopy. *Cell Motility* **49**, 41-47 (2001). https://doi.org:10.1002/cm.1019
36 Kato, H., Nishizaka, T., Iga, T., Kinosita, K. & Ishiwata, S. I. Imaging of thermal activation of actomyosin motors. *Proceedings of the National Academy of Sciences* **96**, 9602-9606 (1999). https://doi.org:10.1073/pnas.96.17.9602
37 Howard, J. Protein power strokes. *Current Biology* **16**, R517-R519 (2006). https://doi.org:https://doi.org/10.1016/j.cub.2006.06.045
38 Ait-Haddou, R. & Herzog, W. Brownian Ratchet Models of Molecular Motors. *Cell Biochemistry and Biophysics* **38**, 191-214 (2003). https://doi.org:10.1385/cbb:38:2:191
39 Astumian, R. D., Mukherjee, S. & Warshel, A. The Physics and Physical Chemistry of Molecular Machines. *ChemPhysChem* **17**, 1719-1741 (2016). https://doi.org:10.1002/cphc.201600184
40 Shin, M. *et al.* Structural basis for distinct operational modes and protease activation in AAA+ protease Lon. *Science Advances* **6**, eaba8404 (2020). https://doi.org:doi:10.1126/sciadv.aba8404
41 Hersch, G. L., Burton, R. E., Bolon, D. N., Baker, T. A. & Sauer, R. T. Asymmetric Interactions of ATP with the AAA+ ClpX6 Unfoldase: Allosteric Control of a Protein Machine. *Cell* **121**, 1017-1027 (2005). https://doi.org:https://doi.org/10.1016/j.cell.2005.05.024

42 Banwait, J. K., Islam, L. & Lucius, A. L. *Single Turnover Transient State Kinetics Reveals Processive Protein Unfolding Catalyzed by Escherichia coli ClpB* (eLife Sciences Publications, Ltd, 2024).
43 Aubin-Tam, M.-E., Olivares, Adrian O., Sauer, Robert T., Baker, Tania A. & Lang, Matthew J. Single-Molecule Protein Unfolding and Translocation by an ATP-Fueled Proteolytic Machine. *Cell* **145**, 257-267 (2011). https://doi.org:https://doi.org/10.1016/j.cell.2011.03.036
44 Lee, Ja Y., Finkelstein, Ilya J., Arciszewska, Lidia K., Sherratt, David J. & Greene, Eric C. Single-Molecule Imaging of FtsK Translocation Reveals Mechanistic Features of Protein-Protein Collisions on DNA. *Molecular Cell* **54**, 832-843 (2014). https://doi.org:https://doi.org/10.1016/j.molcel.2014.03.033
45 Li, T. *et al.* Escherichia coli ClpB is a non-processive polypeptide translocase. *Biochemical Journal* **470**, 39-52 (2015). https://doi.org:10.1042/bj20141457
46 Rosenzweig, R. *et al.* ClpB N-terminal domain plays a regulatory role in protein disaggregation. *Proceedings of the National Academy of Sciences* **112**, E6872-E6881 (2015). https://doi.org:doi:10.1073/pnas.1512783112
47 Rizo, A. N. *et al.* Structural basis for substrate gripping and translocation by the ClpB AAA+ disaggregase. *Nature Communications* **10**, 2393 (2019). https://doi.org:10.1038/s41467-019-10150-y
48 Hänggi, P., Talkner, P. & Borkovec, M. Reaction-rate theory: fifty years after Kramers. *Reviews of Modern Physics* **62**, 251-341 (1990).
49 Makarov, D. E. Computer Simulations and Theory of Protein Translocation. *Accounts of Chemical Research* **42**, 281-289 (2009). https://doi.org:10.1021/ar800128x
50 Amano, S. *et al.* Using Catalysis to Drive Chemistry Away from Equilibrium: Relating Kinetic Asymmetry, Power Strokes, and the Curtin–Hammett Principle in Brownian Ratchets. *Journal of the American Chemical Society* **144**, 20153-20164 (2022). https://doi.org:10.1021/jacs.2c08723
51 Brown, A. I. & Sivak, D. A. Theory of Nonequilibrium Free Energy Transduction by Molecular Machines. *Chemical Reviews* **120**, 434-459 (2020). https://doi.org:10.1021/acs.chemrev.9b00254
52 Wang, H. & Oster, G. Ratchets, power strokes, and molecular motors. *Applied Physics A* **75**, 315-323 (2002). https://doi.org:10.1007/s003390201340
53 Wolfe, A. J., Mohammad, Cheley, S., Bayley, H. & Movileanu, L. Catalyzing the Translocation of Polypeptides through Attractive Interactions. *Journal of the American Chemical Society* **129**, 14034-14041 (2007). https://doi.org:10.1021/ja0749340
54 Sauciuc, A., Morozzo della Rocca, B., Tadema, M. J., Chinappi, M. & Maglia, G. Translocation of linearized full-length proteins through an engineered nanopore under opposing electrophoretic force. *Nature Biotechnology* **42**, 1275-1281 (2024). https://doi.org:10.1038/s41587-023-01954-x
55 Iljina, M. *et al.* Single-molecule FRET probes allosteric effects on protein-translocating pore loops of a AAA+ machine. *Biophysical Journal* **123**, 374-388 (2024). https://doi.org:10.1016/j.bpj.2024.01.002

56 Carusela, M. F. & Rubí, J. M. Entropic rectification and current inversion in a pulsating channel. *The Journal of Chemical Physics* **146**, 184901 (2017). https://doi.org:10.1063/1.4982884

57 Koga, N., Kameda, T., Okazaki, K.-i. & Takada, S. Paddling mechanism for the substrate translocation by AAA+ motor revealed by multiscale molecular simulations. *Proceedings of the National Academy of Sciences* **106**, 18237-18242 (2009). https://doi.org:doi:10.1073/pnas.0904756106

58 Reguera, D. *et al.* Entropic Transport: Kinetics, Scaling, and Control Mechanisms. *Physical Review Letters* **96** (2006). https://doi.org:10.1103/physrevlett.96.130603

59 Astumian, R. D. & Hanggi, P. Brownian motors. *Phys Today* **55**, 33-39 (2002). https://doi.org:Doi 10.1063/1.1535005

60 Tyagi, S. & Lemke, E. A. in *Methods in Cell Biology* Vol. 113 (ed P. Michael Conn) 169-187 (Academic Press, 2013).

61 Akoev, V., Gogol, E. P., Barnett, M. E. & Zolkiewski, M. Nucleotide-induced switch in oligomerization of the AAA+ ATPase ClpB. *Protein Sci* **13**, 567-574 (2004). https://doi.org:10.1110/ps.03422604

62 Schlee, S., Groemping, Y., Herde, P., Seidel, R. & Reinstein, J. The chaperone function of ClpB from Thermus thermophilus depends on allosteric interactions of its two ATP-binding sites11Edited by A. R. Fersht. *Journal of Molecular Biology* **306**, 889-899 (2001). https://doi.org:https://doi.org/10.1006/jmbi.2001.4455

63 Nørby, J. G. in *Methods in Enzymology* Vol. 156 116-119 (Academic Press, 1988).

64 Boukobza, E., Sonnenfeld, A. & Haran, G. Immobilization in surface-tethered lipid vesicles as a new tool for single biomolecule spectroscopy. *Journal of Physical Chemistry B* **105**, 12165-12170 (2001). https://doi.org:10.1021/jp012016x

65 Aitken, C. E., Marshall, R. A. & Puglisi, J. D. An Oxygen Scavenging System for Improvement of Dye Stability in Single-Molecule Fluorescence Experiments. *Biophysical Journal* **94**, 1826-1835 (2008). https://doi.org:10.1529/biophysj.107.117689

66 Heidarsson, P. O. *et al.* Release of linker histone from the nucleosome driven by polyelectrolyte competition with a disordered protein. *Nature Chemistry* **14**, 224-231 (2022). https://doi.org:10.1038/s41557-021-00839-3

67 Ha, T. & Tinnefeld, P. Photophysics of Fluorescent Probes for Single-Molecule Biophysics and Super-Resolution Imaging. *Annual Review of Physical Chemistry* **63**, 595-617 (2012). https://doi.org:10.1146/annurev-physchem-032210-103340

68 Yoo, J., Louis, J. M., Gopich, I. V. & Chung, H. S. Three-Color Single-Molecule FRET and Fluorescence Lifetime Analysis of Fast Protein Folding. *The Journal of Physical Chemistry B* **122**, 11702-11720 (2018). https://doi.org:10.1021/acs.jpcb.8b07768

69 Gopich, I. V. & Szabo, A. Theory of the energy transfer efficiency and fluorescence lifetime distribution in single-molecule FRET. *Proceedings of the National Academy of Sciences* **109**, 7747-7752 (2012). https://doi.org:10.1073/pnas.1205120109